Applied Catalysis B: Environmental 119–120 (2012) 248–255

Contents lists available at SciVerse ScienceDirect

Applied Catalysis B: Environmental

journal homepage: www.elsevier.com/locate/apcatb

Pd and PdAu catalysts supported over 3-MPTES grafted HMS used in the HDS of thiophene

Valeria La Parola, Maria Luisa Testa, Anna Maria Venezia*

Istituto per lo Studio di Materiali Nanostrutturati (ISMN-CNR), via Ugo La Malfa 153, 90146 Palermo, Italy

ARTICLE INFO

Article history:
Received 16 January 2012
Received in revised form 2 March 2012
Accepted 6 March 2012
Available online 13 March 2012

Keywords:
HMS
Mercaptopropyl
PdAu catalysts
HDS
Thiophene

ABSTRACT

Palladium and bimetallic palladium-gold catalysts were supported over mesoporous silica HMS grafted with variable amount of mercaptopropyl groups corresponding to different molar ratio of the —SH group over the metal, $moles_{SH}/moles_{metal}$ = 2, 4, 7, 9. The obtained catalysts, characterized by XRD and XPS techniques were tested in the hydrodesulphurization (HDS) reaction of thiophene. Generally speaking, all the bimetallic catalysts were more active as compared to the monometallic ones. The support modification affected the structure of the fresh (calcined) and reduced catalysts. Supporting the metals over the bare HMS, through deposition–precipitation with urea, produced a drastic decrease of the surface area at variance with the catalysts supported over the functionalized HMS which maintained fairly high surface areas. According to the XRD, the introduction of the —SH groups contributed to the better dispersion of the PdO and metallic gold in the calcined samples. Upon hydrogen treatment the supported metals transformed into small particles of gold enriched alloy leading to high activity and lower catalyst deactivation. The promotion of the catalytic behaviour increased with the increase of the —SH loading up to a molar ratio, $moles_{SH}/moles_{metal}$ = 7. Above this value, the beneficial effect started diminishing. Based on the XPS and the XRD results, the catalytic behaviour was correlated with the structure and surface composition of the supported species, governed by the interaction between the metals and the mercaptogroups.

1. Introduction

Environmental restrictions on the permitted amount of sulphur and aromatics in the transportation fuels, continue to drive the research towards more active and selective hydrotreatment catalysts, with particular attention to the hydrodesulphurization process (HDS) [1,2]. As alternative to the traditional CoMo catalysts, those based on Pd and Pt, have been recently explored [3–5]. As compared to the CoMo catalysts the noble metal ones are more active in the hydrogenation of the aromatics. For this reason they are suitable in "deep" desulphurization, referred to the removal of sulphur from compounds such as dibenzothiophene and alkyl-substituted dibenzothiophenes, particularly refractory to the C—S bond rupture [6]. At variance with the traditional HDS catalysts which are active as sulphides, the palladium and platinum catalysts are active in the metallic state. However during the HDS reaction they become sulphided with consequent loss of activity [4,7]. For this reason their use has been proposed in the so called two-stages system in which a traditional CoMo hydrotreating catalyst is used in the first reactor, in order to decrease the sulphur content to a few parts per million, and a platinum catalyst in the second process to allow for the desulphurization of the refractory compounds at much milder conditions in terms of temperature and hydrogen pressure [8]. Appropriate choice of the support and metal alloying are possible ways for increasing the sulphur tolerance [8–10]. In particular, the acidity of the supports has proven to have a positive effect due to the electron-drawing from the metal particles with the consequent decrease of the interaction between the depleted metal particles and the produced H_2S [7,9]. Decreasing the metal particle size or alloying with another noble metal may attain the same effect, allowing electron depletion and consequent increase of the sulphur tolerance [11]. Recent studies from this laboratory have given indication of a positive effect of gold on the HDS activity of Pd catalysts supported on silica and on amorphous aluminosilicate [3,12]. The beneficial effect of gold, consisting in the inhibition of the less active Pd_4S formation and in a general increase of the catalytic activity, was attributed to Au_xPd_y alloyed particles with consequent geometrical and electronic modification of the active Pd ensemble sites [12]. The extent of the alloy formation and its composition were strongly dependent on the supports and on the catalyst preparation procedures [3,12]. With respect to the supports, differences in the metal–support interaction and in the support

* Corresponding author.
E-mail addresses: venezia@pa.ismn.cnr.it, anna@pa.ismn.cnr.it (A.M. Venezia).

0926-3373/$ – see front matter © 2012 Elsevier B.V. All rights reserved.
doi:10.1016/j.apcatb.2012.03.007

acidity purposely generated by the use of mixed oxides, affected the metal dispersion and therefore the HDS activity [13]. New types of materials have been recently explored as supports for hydrotreatment catalysts. Among these, the ordered mesoporous silicas (e.g., MCM-41, HMS, SBA-15) have attracted much interest due to their high surface area and controlled porosity [14,15]. The silica SBA-15 and silica HMS, functionalized with mercaptopropyl groups, gave rise to a significant enhancement of the HDS activity of the supported CoMo catalysts as compared to the unfunctionalized silica supported catalysts. The effect, more prominent for the HMS series, was explained with the increased reducibility and dispersion of the precursor active species [16]. As a continuation of the previous study, the aim of the present investigation is to extend the use of the support thiol-functionalization to the preparation of HDS catalysts of palladium and bimetallic palladium-gold over silica HMS. The silica was functionalized using the grafting method which, as compared to the so called direct synthesis, was shown to control more efficiently the process of the metal growth [17]. As a preliminary evaluation of the catalytic activity, the reaction of hydrodesulphurization of the thiophene as a function of the metal components and of the atomic ratio, metal to mercapto groups, was considered. The structure and the surface of the materials were characterized by X-ray diffraction (XRD) and X-ray photoelectron spectroscopy (XPS).

2. Experimental

2.1. Support and catalysts preparation

The mesostructured HMS material was synthesized according to a published procedure [18]. Basically, HMS was assembled from 4:1 molar mixtures of tetraethyl orthosilicate (TEOS) (Aldrich) as the inorganic precursor and dodecylamine (DDA) (Aldrich) as the structure-directing surfactant in 9:1 (v/v) water/ethanol. About 49 mmol of DDA were dissolved in 50 ml of ethanol and 450 ml of H_2O. The surfactant solution was heated to 60 °C and 196 mmol of TEOS were added to give the reaction mixture. The gel mixture thus obtained was kept, under stirring, in a closed Teflon vessel at 60 °C for 20 h. The reaction product was filtered, washed with distilled water and dried at room temperature for 24 h. The surfactant was removed by calcination in air at 600 °C for 4 h. The final HMS was modified by grafting procedure. The required amount of 3-mercaptopropyltriethoxysilane (3-MPTES) was added to the activated mesoporous oxide suspended in anhydrous toluene. Anhydrous conditions were indeed important to favour the condensation with the surface sylanol groups. The suspension was kept at 100 °C under reflux overnight. The product was vacuum filtered and washed with toluene and ethanol. Finally it was washed with distilled water to hydrolyse remaining ethoxy groups and then it was dried at 80 °C overnight. The obtained samples were labelled as HMS.*x*SH where *x* (=4, 7, 9) corresponded to the molar ratio between SH and metals.

The monometallic Pd and the bimetallic PdAu catalysts containing 1 wt% Pd and 1 wt% Au were prepared by deposition–precipitation method following the procedure adopted previously with palladium-gold catalysts supported on amorphous aluminosilicate [12]. The relative amount of the two metals was chosen on the bases of the best composition indicated by previous results [3,12]. According to this procedure, urea in a molar ratio of 4:1 with respect to the metals was added to an aqueous suspension of the support containing the dissolved precursor salts $PdCl_2$ and $HAuCl_4{\cdot}3H_2O$ in the appropriate amounts. By heating to 90 °C, the urea decomposed generating OH^- ions precipitating the metal hydroxides on the surface of the support containing —OH and/or —SH groups. The solution at pH ~ 8 was kept refluxing and under stirring for 18 h. Thereafter the suspension was filtered and washed with distilled water. The solid was dried at 60 °C and then calcined at 400 °C for 2 h.

2.2. Catalysts characterization

X-ray diffraction (XRD) analyses were performed with a Bruker goniometer using Ni-filtered Cu Kα radiation. A proportional counter and 0.05° step sizes in 2θ were used. The assignment of the crystalline phases was based on the JPDS powder diffraction file cards [19].

N_2 adsorption–desorption isotherms were measured with a Carlo Erba Sorptomat 1900 instrument. Before the measurements the samples were outgassed at 120 °C for 4 h. The fully computerized analysis of the nitrogen adsorption isotherm at 77 K allowed to estimate the specific surface areas of the samples, through the BET method in the standard pressure range 0.05–0.3 p/p_0. By analysis of the desorption curve, using the BJH calculation method, the pore size distribution was also obtained [20].

The X-ray photoelectron spectroscopy (XPS) analyses were performed with a VGMicrotech ESCA 3000Multilab, equipped with a dual Mg/Al anode. The spectra were excited by the unmonochromatized Al Kα source (1486.6 eV) run at 14 kV and 15 mA. The analyser was operated in the constant analyser energy (CAE) mode. For the individual peak energy regions, a pass energy of 20 eV set across the hemispheres was used. Survey spectra were measured at 50 eV pass energy. The sample powders were analyzed mounted on a double-sided adhesive tape. The samples analysed after reaction were kept in *n*-heptane in order to avoid exposure to air and then transferred into the ion-pumped XPS analysis chamber. The pressure in the analysis chamber was in the range of 10^{-8} Torr during data collection. The constant charging of the samples was removed by referencing all the energies to the C 1s set at 285.1 eV, arising from the adventitious carbon. The invariance of the peak shapes and widths at the beginning and at the end of the analyses ensured absence of differential charging. Analyses of the peaks were performed with the software provided by VG, based on non-linear least squares fitting programme using a weighted sum of Lorentzian and Gaussian component curves after background subtraction according to Shirley and Sherwood [21,22]. Atomic concentrations were calculated from peak intensity using the sensitivity factors provided with the software. The binding energy values are quoted with a precision of ±0.15 eV and the atomic percentage with a precision of ±10%.

2.3. HDS reaction

The hydrodesulphurization of thiophene was carried out in the vapour phase using a continuous flow microreactor [12]. An amount of 200 mg of catalyst (sieved fraction 210–430 mm), diluted with inert particles of SiC (in a weight ratio of 5:1 with respect to the catalyst) was used for each test. The samples were reduced in situ for 2 h in H_2 flow at 50 ml min^{-1} and at 300 °C at a rate of 7 °C min^{-1}). After purging with nitrogen, the HDS of thiophene was carried out at 340 °C with 5.3 vol.% thiophene in H_2 and WHSV = 7500 h^{-1}. The reaction products were analyzed by online gas chromatography (Carlo Erba GC 8340 gaschromatograph). Fractional conversions were calculated from the ratio of the peak area of the C_4 products over the sum of the peak areas of the products and thiophene. The reaction rate for HDS (k_{HDS}) was calculated from the fractional conversion at the steady state conditions, reached after 10 h on stream, assuming a first order reaction in thiophene. A percentage of deactivation (%*d*) was calculated by the differences between the rate at the beginning of the test (after 2 min of time on stream) and the rate at the steady state plateau.

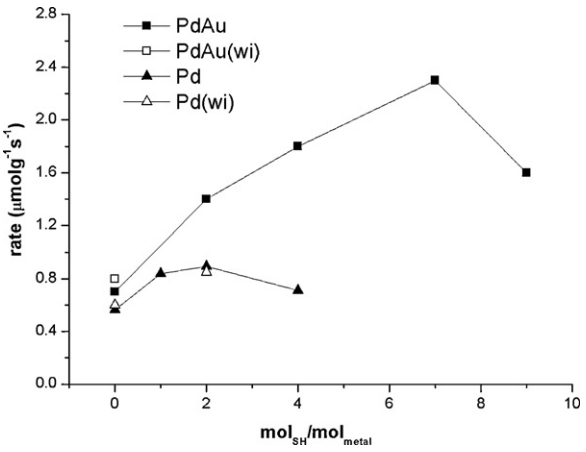

Fig. 1. Thiophene HDS reaction rate as a function of molar ratio between SH and metal mol_{SH}/mol_{metal}. The open symbols refer to catalysts prepared by wet impregnation.

3. Results and discussion

The thiophene HDS reaction rate as a function of the molar ratio between the anchored —SH groups and the total metal atoms are plotted in Fig. 1 for the two series of the monometallic and bimetallic catalysts. For comparison reason to be discussed later, data from similar catalysts prepared by wet impregnation are also included. In Table 1 the conversion and the percentage of deactivation are summarized. As already reported for the palladium and the bimetallic PdAu catalysts supported over pure silica and pure aluminosilicates [3,12], the promoting effect of gold is here confirmed also for the bare HMS supported catalysts, for which a slightly better activity for the bimetallic catalysts as compared to the monometallic is observed. It should be reminded that the previous study on the thiophene HDS activity of bimetallic PdAu supported catalysts ascertained the superior catalytic activity of the gold enriched alloy particles as compared to pure palladium or palladium enriched alloy particles [12].

Regarding the functionalized supports, the —SH loading has clearly a different effect over the two series of samples. The activity of the monometallic palladium catalyst is not much modified within the range of —SH to metal molar ratio between 1 and 4. On the contrary, a five times increase of the activity is attained in the bimetallic series. For these samples the enhancement of the activity proceeds even for larger molar ratios, $moles_{SH}/moles_{Metal}$, reaching a maximum in correspondence of the ratio equal to 7, thereafter diminishing. As listed in Table 1, deactivation percentages of the monometallic catalysts are not significantly affected by the functionalization of the support. On the contrary, with the exception of the PdAuHMS_9SH, the bimetallic catalysts over the —SH modified supports deactivate less as compared to the homologous one on bare HMS.

Table 1
Thiophene conversion (χ) at 340 °C and percentage of deactivation (d%) of the supported mono and bi-metallic catalysts.

Catalysts[a]	χ	d (%)
PdHMS	0.05	21
PdHMS_2SH	0.08	20
PdHMS_4SH	0.07	25
PdAuHMS	0.07	25
PdAuHMS_4SH	0.17	12
PdAuHMS_7SH	0.22	16
PdAuHMS_9SH	0.16	26

[a] In the catalyst notation HMS_xSH, x (=4, 7, 9) corresponds to the molar ratio between SH and metals.

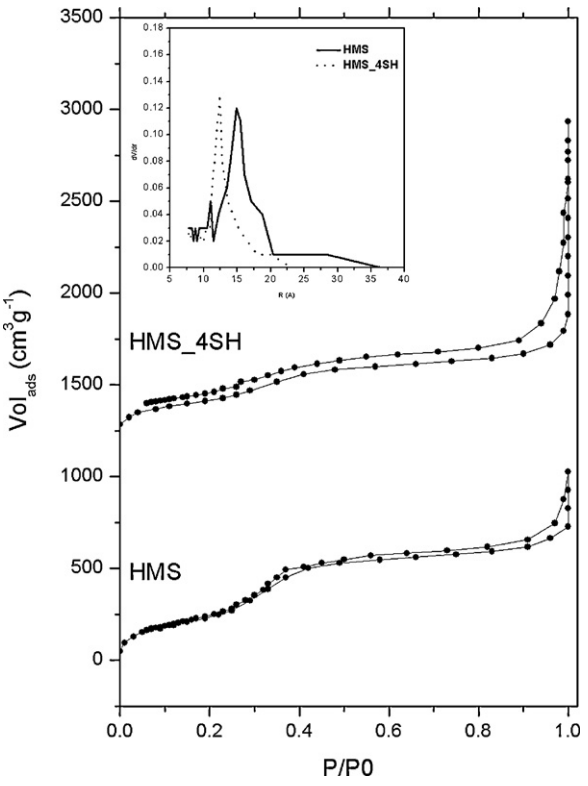

Fig. 2. N_2 adsorption–desorption isotherms of pure HMS and functionalized HMS_4SH. The pore size distributions are shown in the inset.

The nitrogen adsorption–desorption isotherms of pure HMS and of functionalized HMS_4SH are shown in Fig. 2. The isotherms are of type IV [20,23]. In both supports the hysteresis loops are rather flat and extended over a large range of relative pressures, indicating the presence of both framework meso-porosity and interparticle macro-porosity [24]. As shown in the figure, the introduction of the mercaptogroups induces a flattening of the hysteresis loop. In Table 2 the textural properties of the two selected supports and of the bimetallic catalysts are summarized. As reported previously and in analogy with what observed on similarly functionalized amorphous silica, the grafted HMS_4SH sample undergoes a decrease of the original surface area and of the average pore size [17,25]. Concerning the bimetallic catalysts, they are characterized by still high surface areas and larger average pore sizes as compared to the HMS. As a general trend, as indicated in Table 2 by the surface area difference between the PdAuHMS_4SH and the HMS_4SH, the deposition of the metals produces a certain lowering of the surface area with respect to the corresponding supports. On the contrary, in the case of the catalyst supported over the bare HMS, the metal deposition causes a drastic decrease of the surface area. The value obtained for this catalyst is in contrast with the much larger area of a previous PdAu catalyst over HMS

Table 2
Specific surface area (S_{BET}) and average pore size (D_p).

Catalysts	S_{BET} [a] (m^2/g)	D_p [a] (nm)
HMS	927	3
HMS_4SH	858	2.4
PdAuHMS	100	3.6
PdAuHMS_4SH	523	3.5
PdAuHMS_7SH	346	3.4
PdAuHMS_9SH	364	3.5

[a] The specific surface area and the average pore diameters were calculated from N_2 adsorption–desorption isotherms.

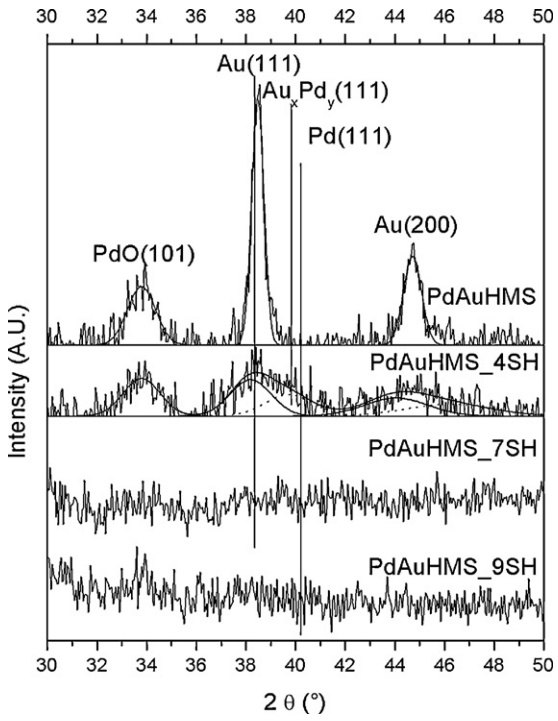

Fig. 3. XRD patterns of calcined bimetallic PdAu catalyst supported over-*x*SH modified HMS.

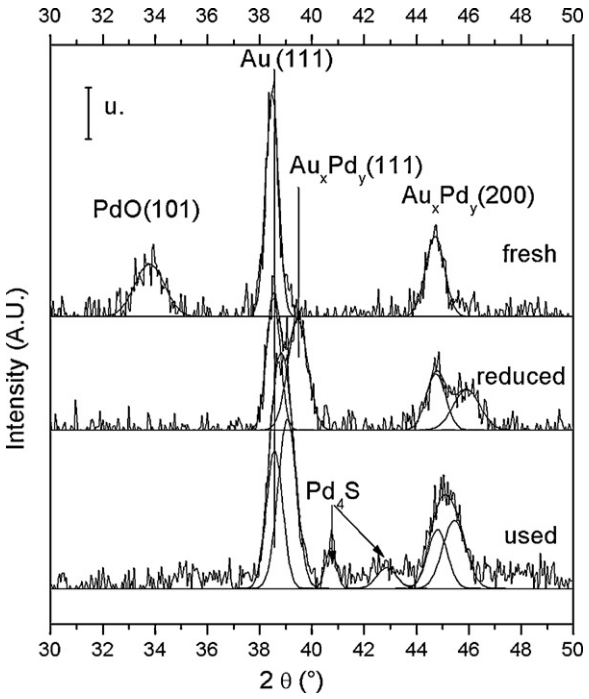

Fig. 4. XRD patterns of fresh, reduced and used PdAu_HMS catalyst.

exhibiting only a 20% decrease with respect to the corresponding support [26]. According to the literature, one problem related to the use of this type of mesoporous materials is the poor hydrothermal stability [27]. The previously reported PdAuHMS catalysts prepared by wet impregnation with $PdCl_2$ and $AuCl_3$ aqueous solutions [26] maintained the structure and the large surface area of 670 m^2/g of the mesoporous support. Here, on the contrary, the basic condition (pH = 8) attained during the deposition–precipitation of the present catalysts, most likely contributes to the collapse of the mesopores with consequent loss of the surface area, as a result of the silicate hydrolysis [28]. The presence of the propylmercaptogroups obviously avoids or limits such pH related effect. In order to check the support structure influence on the catalytic activity, three selected catalysts prepared by wet impregnation on bare and on functionalized HMS were also tested in the HDS of thiophene and included in Fig. 1. Their catalytic activities fit very well the data of the catalyst series obtained with the urea method. Based on this comparison, the activity promotion observed in the HMS_*x*SH supported catalyst is mainly ascribable to the effect of the functional group, notwithstanding the drastic decrease of the surface area.

The ordered mesoporous structure of the HMS was confirmed by the small angle X-ray diffraction pattern, exhibiting the typical peak near 2.2° 2θ [23]. Grafting with the propyl-SH moieties produced a decrease of the intensity of the peak which totally disappeared in the supported catalysts, proving the loss of the mesostructure order [16,17].

The structure of the catalysts at different life stages was investigated by X-ray diffraction analyses. The samples were analysed in the fresh (calcined) state, after reduction in hydrogen and after catalytic reaction. The X-ray diffraction patterns of the calcined monometallic PdHMS and PdHMS_*x*SH samples are not shown since they did not contain any peaks, suggesting amorphous phases or crystallites sizes smaller than the detection limit of 2 nm. On the contrary, as shown in Fig. 3, the patterns of the calcined bimetallic catalysts exhibit crystalline features, the intensity of which depends on the functional group loading. Moreover, support modification produces a quite remarkable effect on the metal dispersion. In the PdAuHMS sample, along with the broad PdO(1 0 1) reflection, narrower peaks located in correspondence of the metallic Au(1 1 1) and Au(2 0 0) reflections are present. In the catalysts over the −4SH modified support the intensity of the PdO(1 0 1) peak decreases and at the same time the peaks related to the metallic Au species become weaker, broader and with asymmetry towards the position of the metallic Pd(1 1 1) reflection, shown in the figure as reference. Using a peak fit routine, the feature ranging from 36° to 40° 2θ is decomposed into two components, one attributed to the pure gold and the other to a palladium enriched alloy. From the lattice parameter shifts, calculated from the angular position of the high 2θ component of the (1 1 1) metal reflection, according to Vegard's law, the molar compositions *x* and *y* of the solid solutions Au_xPd_y are roughly estimated [29]. The particle sizes of the different crystalline phases are calculated from the line broadening of the most intense reflections using the Scherrer equation [30]. The results of these calculations are summarized in Table 3. Comparing the data for the fresh catalyst over bare HMS and the fresh catalyst over HMS_4SH, it is quite evident how the presence of the −SH groups in the support gives rise to smaller crystalline particles particularly for the gold and alloy particles. The other fresh samples derived from higher −SH loaded supports are completely amorphous. The XRD patterns of the bimetallic catalysts supported over pure HMS and over the −4SH loaded HMS after reduction and after hydrodesulphurization reaction are shown in Figs. 4 and 5 respectively. In both figures, the diffractograms of the fresh samples, reported already in Fig. 3, are shown again for easier comparison. According to the patterns of Fig. 4, the reduction treatment of PdAuHMS causes the disappearance of the PdO crystallites, the permanence of gold particles and the formation of alloy particles enriched in palladium. After the catalytic reaction, particles of gold and of slightly gold enriched alloy are present in the sample along with particles of Pd_4S which were already reported to be less active as compared to metallic Pd [12]. According to the patterns of −4SH modified HMS supported catalysts, shown in Fig. 5, the PdO phase disappears. As indicated by the corresponding values in Table 3, quite well dispersed alloy particles significantly enriched

Table 3
Chrystal phases of the mono and bimetallic samples after different stages.

Samples	Crystal phases	Particle diameters (nm)
PdAuHMS fresh	PdO	6.8
	Au	16.1
PdAuHMS reduced	Au	10
	$Au_{36}Pd_{64}$	15
PdAuHMS used	Au	12
	$Au_{57}Pd_{43}$	14
	Pd_4S	10
PdAuHMS_4SH	PdO	5.2
	Au	5
	$Au_{25}Pd_{75}$	4
PdAuHMS_4SH reduced	$Au_{72}Pd_{28}$	2
PdAuHMS_4SH used	$Au_{72}Pd_{28}$	2
PdAuHMS_7SH	traces PdO	
PdAuHMS_7SH reduced	$Au_{60}Pd_{40}$	2
PdAuHMS_9SH	traces PdO	
PdAuHMS_9SH reduced	$Au_{60}Pd_{40}$	2

in gold are formed in both cases, after reduction and after catalytic reaction. Along with the much better dispersion of the alloy phases, functionalization of the HMS with mercapto groups seems to prevent the formation of the Pd_4S species. In Fig. 6 the patterns relative to the reduced bimetallic catalysts supported over the HMS with higher $mol_{SH}/mol_{met\ in}$ are shown. As reported in Table 3, fitting of the peaks yields gold enriched alloy particles with similar composition and similar size for both samples. From a qualitatively point of view, relatively to PdAuHMS_9SH it is worth noticing the slightly larger width, with an asymmetry on the high angle side, indicative of the presence of an additional phase of palladium enriched alloy. Given the low signal to noise ratio, attempts of fitting with free parameters were not successful and the calculated value of the alloy composition would have not been reliable.

The oxidation state of palladium and gold and the elemental distribution on the catalyst surface at different stages of its life was investigated by photoelectron spectroscopy. The experimental Au 4f spectra and the Pd 3d spectra are shown respectively in Figs. 7 and 8 along with the fitted curves for selected bimetallic catalysts. The gold spectra are characterized by the two spin orbit components Au $4f_{7/2}$ and Au $4f_{5/2}$ and the palladium spectra by the two spin orbit components Pd $3d_{5/2}$ and Pd $3d_{3/2}$. The Au $4d_{5/2}$ peak overlapping with the Pd $3d_{5/2}$ region has also been fitted and it is represented by the dashed curve. For the fitting of this peak its energy and intensity constraints with the Au $4d_{3/2}$ component, lying at higher binding energy and not shown in the figure, were considered [3]. Figs. 7 and 8 contain two panels, each referring to the bimetallic catalysts supported over bare HMS and over HMS_4SH. Purposely, the reported energy range of the Au 4f includes also the X-ray satellite peak of the Si 2p. The variation

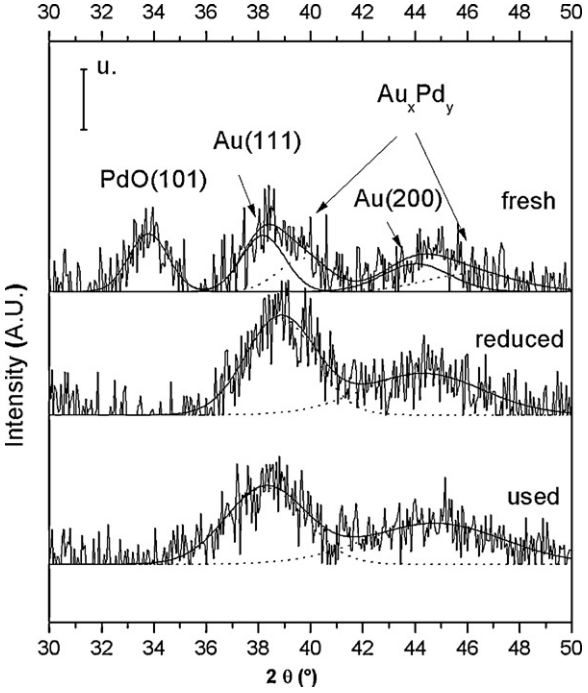

Fig. 5. XRD patterns of fresh, reduced and used PdAuHMS_4SH catalyst.

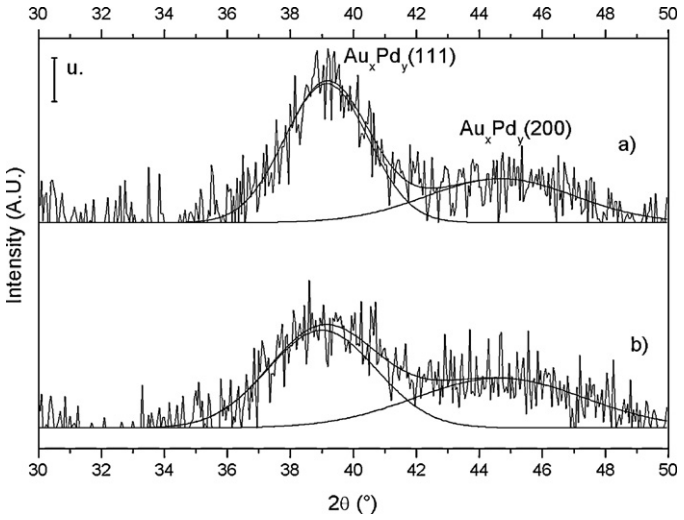

Fig. 6. XRD patterns of reduced: (a) PdAuHMS_7 SH; (b) PdAuHMS_9 SH.

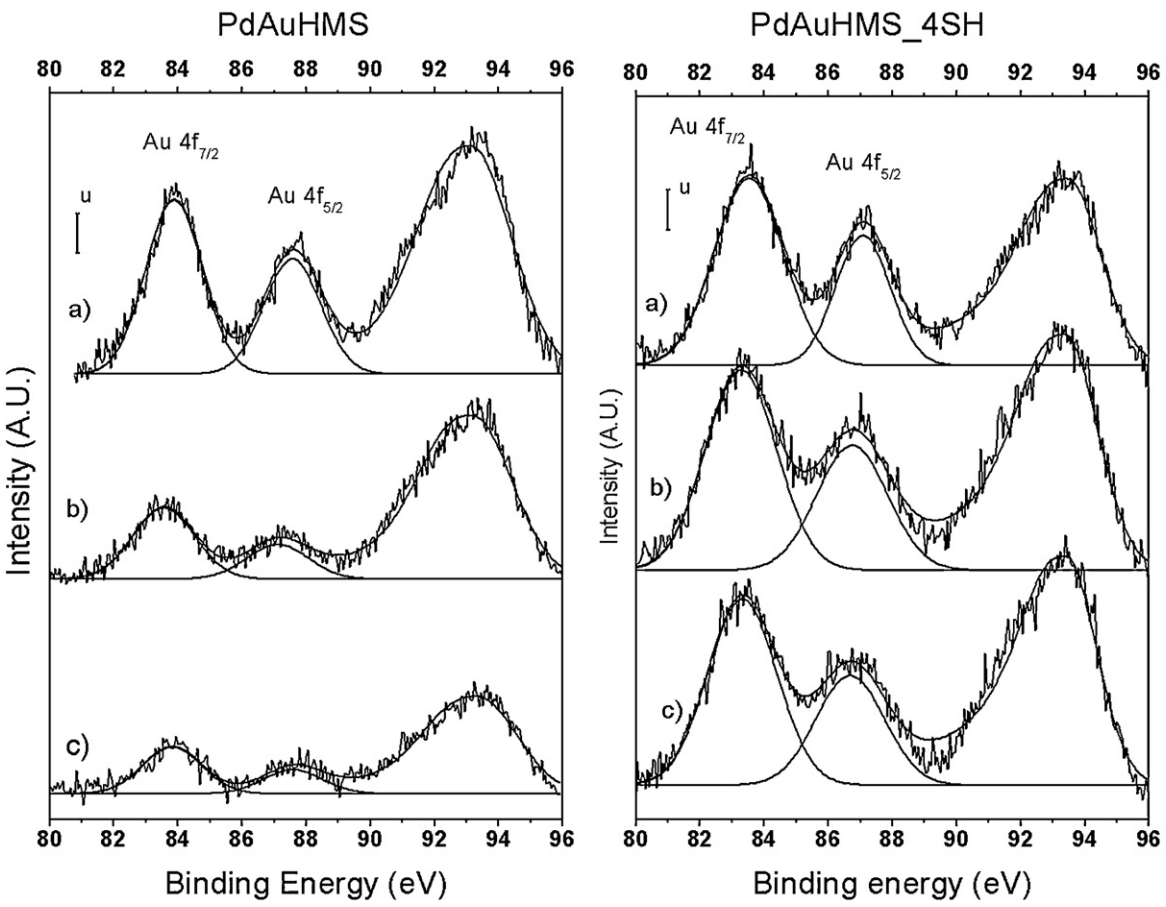

Fig. 7. Au 4f XP spectra of bimetallic catalysts as: (a) fresh; (b) reduced; (c) aged.

of the intensity of the gold peaks with respect to the intensity of the silicon satellite peak probes directly the surface compositional changes at different catalyst stages. From the reported spectra it is evident how in the absence of functionalization, the surface gold concentration in PdAuHMS changed with respect to silica, differently from the PdAuHMS_4SH exhibiting stable gold concentration after the different stages. The results from the XPS analyses are summarized in Table 4 in terms of binding energies and atomic ratios. According to the binding energy values and to the spectra in Fig. 7, no significant changes in Au 4f binding energies occurred upon different sample treatments. Moreover, no substantial differences are envisaged between the Au $4f_{7/2}$ binding energy

Table 4
XPS Pd $3d_{5/2}$, Au $4f_{7/2}$ binding energies and atomic ratios of the catalysts as fresh, after hydrogen reduction (*a.r.*) and after catalytic HDS reaction ($a.r_{HDS}$).

Samples	Pd $3d_{5/2}$ (eV)	Au $4f_{7/2}$ (eV)	Pd/Si(0.005)[a]	Au/Si(0.003)[a]	Pd/Au(1.8)[a]
PdHMS	336.0		0.005		
PdHMS *a.r.*	334.9		0.005		
PdHMS $a.r_{HDS}$.	335.3		0.004		
PdHMS_1SH	335.7		0.004		
PdHMS_2SH	335.6		0.004		
PdHMS_4SH	335.8		0.006		
PdHMS_4SH *a.r.*	334.8		0.004		
PdAuHMS	334.9 (29%)	83.9	0.001	0.003	0.3
	336.8 (71%)				
PdAuHMS *a.r.*	335.0	83.5	0.002	0.002	1.0
PdAuHMS $a.r_{HDS}$	335.5	83.8	0.002	0.002	1.0
PdAuHMS_4SH	334.6 (43%)	83.5	0.005	0.005	1.0
	336.4 (57%)				
PdAuHMS_4SH *a.r.*	334.6	83.3	0.004	0.004	1
PdAuHMS_4SH $a.r_{HDS}$	334.8	83.3	0.003	0.004	0.8
PdAuHMS_7SH	334.7 (68%)	83.6	0.006	0.007	0.9
	336.1 (32%)				
PdAuHMS_7SH *a.r.*	334.7	83.3	0.005	0.006	0.8
PdAuHMS_9SH	334.9 (70%)	83.8	0.003	0.007	0.4
	336.3 (30%)				
PdAuHMS_9SH *a.r.*	335.0	83.6	0.009	0.008	1.1
PdAuHMS_9SH $a.r_{HDS}$	335.1	83.5	0.004	0.005	0.8

[a] These numbers represent the nominal values.

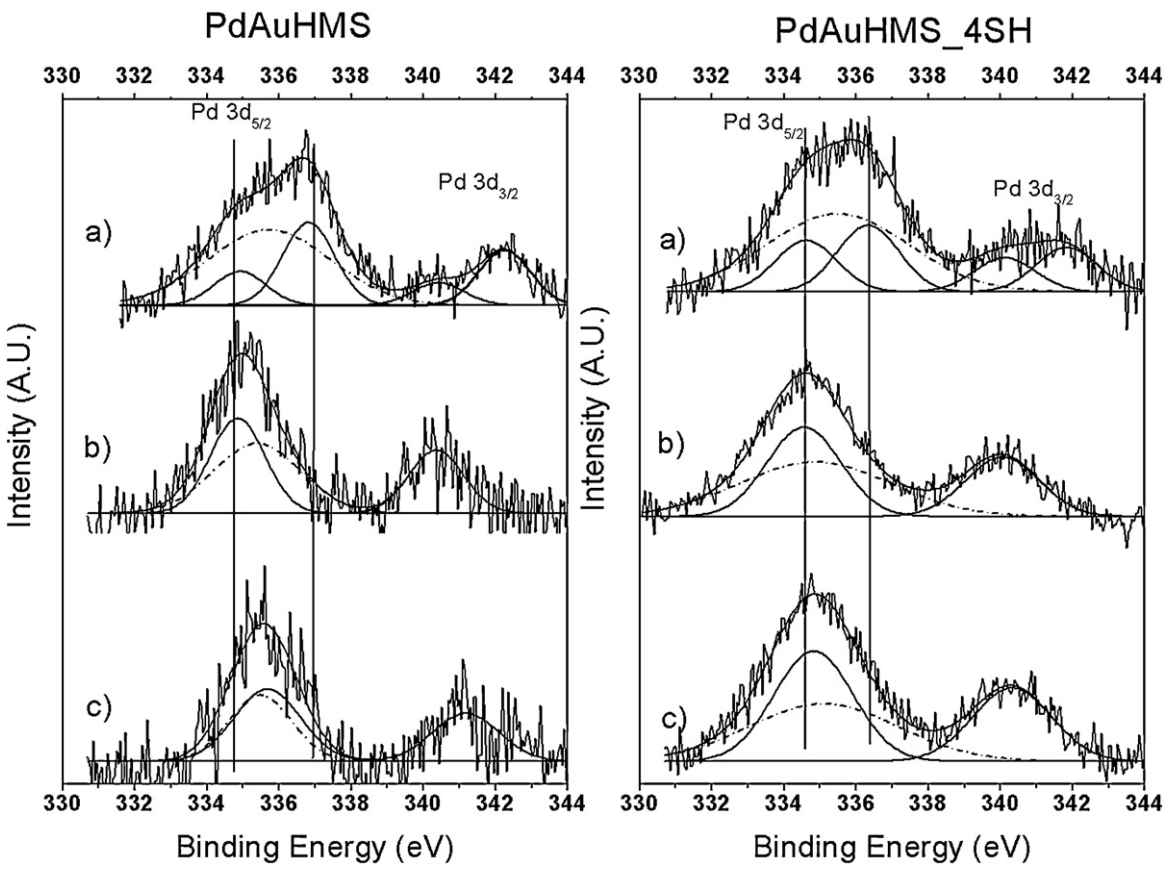

Fig. 8. Pd 3d XP spectra of bimetallic catalysts as: (a) fresh; (b) reduced; (c) aged.

of the catalyst supported over the bare HMS and of the catalyst over the —SH functionalized support. With respect to the Pd 3d binding energies, as shown in Table 4, differences exist between the calcined (fresh) monometallic and the bimetallic catalysts. In the calcined monometallic catalysts the Pd $3d_{5/2}$ core level has a binding energy of 335.8 eV ± 0.2 eV typical of Pd^{2+}. In the case of the bimetallic catalysts, in accord with the XRD detection of alloy phases, the Pd 3d spectra was fitted with two components, one at lower energy (334.8 eV ± 0.2) attributed to metallic Pd and the other at higher binding energy attributed to PdO. As seen in Fig. 8, the two components are present also in the catalyst without support functionalization. The effect of gold in promoting the reduction of palladium was already reported for PdAu bimetallic catalysts supported over amorphous silica and alluminosilicate [3,12]. As indicated in Table 4, the percentage of the metallic component increases with the support —SH loading. As shown in the table and in Fig. 8 for the PdAuHMS and the PdAuHMS_4SH, the reduction treatment with H_2 and the catalytic reaction both cause the disappearance of the Pd 3d oxide component. A Pd $3d_{5/2}$ positive binding energy shift of 0.7 eV is observed for the PdAuHMS after catalytic reaction with respect to the sample after hydrogen reduction. Such energy change could be attributed to the presence of Pd_4S species formed during the HDS reaction and detected in the XRD pattern of the aged sample. Quite interestingly, no XPS chemical shift is found for the PdAuHMS_4SH, in accord with the lack of XRD evidence for Pd_4S. As clearly indicated in Table 4, variation of the XPS derived atomic ratios are observed between the samples at the different stages. The catalyst PdAuHMS, characterized by the smallest Pd/Au atomic ratio in the fresh state, is the one exhibiting the largest Au/Si and Pd/Au atomic ratio changes upon sample treatments, with a substantial increase of the Pd/Si ratio. For this sample, according to the increasing of the Pd/Au and Pd/Si and the lowering of the Au/Si ratios, surface migration of palladium is driven by the reduction treatment. On the contrary, no significant changes of the Pd/Au atomic ratio with a slight decrease of the metal to silicon ratios are observed in PdAuHMS_4SH in the different stages. Stable surface distributions of both metal species are observed also in the reduced PdAuHMS_7SH sample with respect to the fresh state. In the case of the high —SH support loaded catalyst PdAuHMS_9SH, the variations of the Pd/Au atomic ratio after reduction and after reaction are similar to those observed for the sample over the bare HMS and in accord with palladium migration to the catalyst surface. Moreover similar values of Pd $3d_{5/2}$ binding energy are obtained for the reduced PdAuHMS and the PdAuHMS_9SH samples. In spite of this similarity, larger Pd/Si and Au/Si ratios obtained for the reduced and aged PdAuHMS_9SH indicate better surface metal dispersion as compared to the PdAuHMS sample, justifying the better activity of the former sample. As discussed above, from the structural point of view the two catalysts PdAuHMS_7SH and PdAuHMS_9SH are similar, with supposedly well dispersed metal species, not evidenced in the amorphous XRD pattern of the calcined samples, and with aggregation of gold enriched Au_xPd_y alloy particles after reduction (Fig. 6). However, the decreased activity of the PdAuHMS_9SH as compared to the PdAuHMS_7SH, on the bases of the XPS analysis, can be correlated with the different surface chemical composition of the supported species.

According to the XPS and XRD results, the functionalization of the silica support affects the structure of the reduced bimetallic catalysts in a way which is related to the amount of propyl-SH groups grafted to the support. During the metal deposition–precipitation with urea, a competition between the interaction of the metal with the thiol and with the sylanol groups is likely taking place. On the basis of the solubility constants of $Au(OH)_3$ and $Pd(OH)_2$ which are equal to 3×10^{-6} and 3×10^{-30} respectively [12], and in the

absence of —SH groups, it is expected that under the pH conditions established by decomposition of urea, palladium hydroxide would precipitate first, anchoring to the surface sylanols, producing small palladium particles. Gold would precipitated far from the support with the formation of large particles of gold and/or eggshell particles. According to the deposition–precipitation mechanism the inner core of the eggshell particle would be made of palladium oxide and the topmost layer made of gold explaining the XRD and the XPS Pd/Au atomic ratio of the calcined PdAuHMS sample. Upon reduction and subsequent catalytic reaction, the structure of the particles would change due to palladium migration. A more homogeneous chemical composition with formation of bimetallic alloy particles enriched in palladium having the large size of the calcined precursors would form. In the presence of —SH, given the good interaction between Pd—S and Au—S, both metals would anchor to the surface yielding, after calcinations, smaller PdO, Au and Au_xPd_y particles. After reduction, small alloy particles enriched in gold and stable under the reaction conditions are obtained with consequent increase of the activity as compared to the bare HMS supported catalyst. This positive effect increases with the amount of —SH groups, ranging from an amount of —SH in defect with respect to the stoichiometric amount required to bind the metals (corresponding to SH/M = 5, considering Pd^{2+} bound to two —SH and Au^{3+} bound to 3 —SH) to an amount in slight excess. The presence of a large number of —SH groups, such as in the PdAuHMS_9SH, still contributes to the good dispersion of gold and palladium during the calcination stage. However, since —SH groups replace the OH groups of the support, palladium and gold will compete both with SH and in virtue of the stronger Pd—S bond (∼175 kcal/mol [31]) as compared to the Au—S (Au—S = 60 kcal/mol [32]) again an eggshell structure with a palladium core is likely formed. As indicated by the XPS Pd/Au atomic ratio, migration of palladium towards the catalyst surface must take place during the reduction treatment. As suggested by the asymmetry of the XRD peak of this particular sample, some palladium enriched alloy particles are formed as well and the catalyst starts to behave as the non functionalized catalyst. Therefore, decrease of the activity and increase of the percentage of deactivation due to the Pd_4S formation are observed. In other words, due to the SH groups the good dispersion of the metallic particles is maintained, however the chemical composition of the active particle is getting closer to that of a monometallic palladium catalyst or of the bimetallic over the bare HMS.

4. Conclusion

Functionalization of the HMS support with mercaptopropyl groups has a negligible effect on the thiophene HDS activity of the supported monometallic palladium catalysts, whereas it has a significantly positive effect on the activity of the bimetallic palladium-gold catalysts.

The beneficial effect increases with the mercapto group loading up to a certain amount, thereafter starting to decrease. Based on XRD and XPS analyses, the promotion of the activity in the —SH modified HMS supported catalysts is correlated with the following structural modifications: (i) increase of the dispersion of both metal species, as proven by the broadening or by the absence of the related XRD peaks of the calcined samples; (ii) formation of the more active dispersed gold enriched alloyed particles, during the hydrogen-pretreatment; (iii) increased stability of the particle chemical composition and dimension, as shown by the invariance of the XRD pattern and XPS atomic ratio Pd/Au after the reduction and the catalytic test; (iv) decrease of the catalyst deactivation by inhibiting the formation of the less active Pd_4S species during reaction.

The main reason for these structural effects is plausibly related to different interaction of the metal precursors with the surface —OH and —SH groups. From the practical point of view, an important result of this investigation is the possibility of modifying the particle structure of a bimetallic PdAu system by fine tuning the molar ratio between the —SH groups and the total sum of the two metals (—SH/M).

Acknowledgement

Support by the European Community, COST Action CM0903 is acknowledged.

References

[1] EP directive 2003/17/EC, Off. J. Eur. Union L 76, 46 (2003) 10.
[2] C. Song, Catal. Today 86 (2003) 211–263.
[3] A.M. Venezia, V. La Parola, G. Deganello, B. Pawelec, J.L.G. Fierro, J. Catal. 215 (2003) 317–325.
[4] Y. Sun, H. Wang, R. Prins, Catal. Today 150 (2010) 213–217.
[5] E.W.Q.K. Otani, L. Li, A. Ishihara, T. Kabe, J. Catal. 221 (2004) 294–301.
[6] R. Prins, in: G. Ertl, H. Knozinger, F. Schüth, J. Weitkamp (Eds.), Handbook of Heterogeneious Catalysis, vol. 6, 2nd ed., Wiley-VCH, Weinheim, 2008, p. 2695.
[7] L.J. Simon, J.G. Van Ommen, A. Jentys, J.A. Lercher, J. Catal. 203 (2001) 434–442.
[8] C. Song, Chemtech 29 (1999) 26–30.
[9] A.M. Venezia, R. Murania, V. La Parola, B. Pawelec, J.L.G. Fierro, Appl. Catal. 383 (2010) 211–216.
[10] M.M. Hossain, Chem. Eng. J. 123 (2006) 15–23.
[11] R.M. Navarro, B. Pawelec, J.M. Trejo, R. Mariscal, J.L.G. Fierro, J. Catal. 189 (2000) 184–194.
[12] A.M. Venezia, V. La Parola, V. Nicolì, G. Deganello, J. Catal. 212 (2002) 56–62.
[13] Z. Gu, L. Luo, M. Teng, Ind. J. Chem. 46A (2007) 742–747.
[14] A. Corma, A. Martinez, V. Martinez-Soria, J. Catal. 169 (1997) 480–489.
[15] T.A. Zepeda, B. Pawelec, J.L.G. Fierro, A. Olivas, S. Fuentes, T. Halachev, Micropor. Mesopor. Mater. 111 (2008) 157–170.
[16] V. La Parola, B. Dragoi, A. Ungureanu, E. Dumitriu, A.M. Venezia, Appl. Catal. A (2010) 43–50.
[17] V. La Parola, A. Longo, A.M. Venezia, A. Spinella, E. Caponetti, Eur. J. Inorg. Chem. (2010) 3628–3635.
[18] J. Brown, L. Mercier, T.J. Pinnavaia, Chem. Commun. (1999) 69–70.
[19] JCPDS Powder Diffraction File, Int. Centre for Diffraction Data, Swarthmore, 1989 (File No. 42-1467).
[20] S.J. Gregg, K.S. Sing, Adsorption, Surface Area and Porosity, 2nd ed., Academic Press, San Diego, 1982.
[21] D.A. Shirley, Phys. Rev. B 5 (1972) 4709–4714.
[22] P.M.A. Sherwood, in: D. Briggs, M.P. Seah (Eds.), Practical Surface Analysis, Wiley, New York, 1990, p. 181.
[23] N. Marin-Astorga, G. Pecchi, T.J. Pinnavaia, G. Alvez-Manoli, P. Reyes, J. Mol. Catal. A 247 (2006) 145–152.
[24] R. Nava, B. Pawelec, J. Morales, R.A. Ortega, J.L.G. Fierro, Micropor. Mesopor. Mater. 118 (2009) 189–201.
[25] M.L. Testa, V. La Parola, A.M. Venezia, Catal. Today 158 (2010) 109–113.
[26] A.M. Venezia, R. Murania, G. Pantaleo, G. Deganello, J. Catal. 251 (2007) 94–102.
[27] A. Doyle, B.K. Hodnett, Micropor. Mesopor. Mater. 63 (2003) 53–57.
[28] R. Ryoo, S. Jun, J. Phys. Chem. B 101 (1997) 317–320.
[29] A.R. West, Solid State Chemistry and its Applications, John Wiley and Sons Ltd., Chichester, England, 1998.
[30] H.P. Klug, L.E. Alexander, X-ray Diffraction Procedures for Polycrystalline and Amorphous Materials, Wiley, New York, 1954.
[31] H.H. Toulhoat, P. Raybaud, S. Kasztelan, G. Kresse, J. Hafner, Catal. Today 50 (1999) 629–636.
[32] P. Pyykkö, X.-G. Xiong, J. Li, Faraday Discuss. 152 (2011) 169–178.